Parallel β-Sheets and Polar Zippers in Amyloid Fibrils Formed by Residues 10−39 of the Yeast Prion Protein Ure2p

Jerry C. C. Chan,‡ Nathan A. Oyler, Wai-Ming Yau, and Robert Tycko*

Laboratory of Chemical Physics, National Institute of Diabetes and Digestive and Kidney Diseases, National Institutes of Health, Bethesda, Maryland 20892-0520

Received April 19, 2005; Revised Manuscript Received June 16, 2005

ABSTRACT: We report the results of solid-state nuclear magnetic resonance (NMR) and atomic force microscopy measurements on amyloid fibrils formed by residues 10−39 of the yeast prion protein Ure2p (Ure2p$_{10-39}$). Measurements of intermolecular $^{13}C-^{13}C$ nuclear magnetic dipole−dipole couplings indicate that Ure2p$_{10-39}$ fibrils contain in-register parallel β-sheets. Measurements of intermolecular $^{15}N-^{13}C$ dipole−dipole couplings, using a new solid-state NMR technique called DSQ-REDOR, are consistent with hydrogen bonds between side chain amide groups of Gln18 residues. Such side chain hydrogen bonding interactions have been called "polar zippers" by M. F. Perutz and have been proposed to stabilize amyloid fibrils formed by peptides with glutamine- and asparagine-rich sequences, such as Ure2p$_{10-39}$. We propose that polar zipper interactions account for the in-register parallel β-sheet structure in Ure2p$_{10-39}$ fibrils and that similar peptides will also exhibit parallel β-sheet structures in amyloid fibrils. We present molecular models for Ure2p$_{10-39}$ fibrils that are consistent with available experimental data. Finally, we show that solid-state ^{13}C NMR chemical shifts for ^{13}C-labeled Ure2p$_{10-39}$ fibrils are insensitive to hydration level, indicating that the fibril structure is not affected by the presence or absence of bulk water.

One goal of current efforts to elucidate the molecular structures of amyloid fibrils (*1*−*35*) is to identify the intermolecular interactions that determine the details of these structures and make amyloid fibrils a stable structural state for many peptides and proteins despite their diversity of amino acid sequences (*36*−*41*). Recent studies by solid-state nuclear magnetic resonance (NMR)[1] of fibrils formed by the β-amyloid (Aβ) peptide associated with Alzheimer's disease (*5*, *13*, *16*, *18*, *24*, *30*, *31*), by various Aβ fragments (*1*, *3*, *4*, *6*−*8*, *12*, *21*, *25*), and by other amyloid-forming peptides (*22*) indicate that the β-sheets in amyloid fibrils have structures that tend to maximize contacts among hydrophobic residues when the component peptides contain continuous hydrophobic segments. Electrostatic interactions appear to play a secondary role, dictating the choice between parallel and antiparallel β-sheet structures when either type of structure could maximize hydrophobic contacts (*6*, *21*, *23*) and dictating the precise registry of intermolecular hydrogen bonds in antiparallel β-sheets (*1*, *25*). Electrostatic repulsions in the low-dielectric core of an amyloid fibril could in principle overwhelm the favorable hydrophobic interactions and thus destabilize the amyloid structure (*16*). However, amyloid-forming peptides have been found to adopt conformations and supramolecular organizations that prevent electrostatic repulsions in the core (*6*, *16*, *23*, *25*). These conclusions from solid-state NMR data are supported by structural data from other sources, including electron paramagnetic resonance (*17*, *19*, *42*), proline-scanning mutagenesis (*28*), disulfide cross-linking (*26*), chemical derivatization (*21*), and X-ray diffraction (*29*).

Amyloid fibrils formed by peptides and proteins that lack hydrophobic segments may be stabilized by different sets of interactions. Peptides and protein segments that are rich in glutamine or asparagine residues are of particular interest, both because of their involvement in neurodegenerative disorders such as Huntington's disease (*43*, *44*) and spinocerebellar ataxias (*45*) and because of their occurrence in amyloid-forming yeast prion proteins (*46*−*50*). The propensity for glutamine- and asparagine-rich peptides and proteins to aggregate as amyloid fibrils in aqueous solutions [which may be surprising, given that glutamine and asparagine are not generally considered to be highly hydrophobic (*51*, *52*)] led Perutz to propose that these fibrils are stabilized by linear chains of hydrogen bonds among the amide groups of glutamine and asparagine side chains on neighboring β-strands within a single β-sheet layer. Perutz coined the phrase "polar zippers" to describe the putative side chain hydrogen bonding interactions (*43*, *53*−*56*). Molecular modeling indicates the feasibility of polar zipper formation in amyloid fibrils (*45*, *53*); side chain hydrogen bonds among asparagine residues in neighboring β-strands have been observed in protein crystal structures (*57*−*59*), and experimental constraints on the conformations of polyglutamine peptides in amyloid

* To whom correspondence should be addressed: National Institutes of Health, Building 5, Room 112, Bethesda, MD 20892-0520. Phone: (301) 402-8272. Fax: (301) 496-0825. E-mail: robertty@mail.nih.gov.

‡ Current address: Department of Chemistry, National Taiwan University, Taipei, Taiwan.

[1] Abbreviations: NMR, nuclear magnetic resonance; Aβ, β-amyloid peptide; Ure2p$_{10-39}$, residues 10−39 of the Ure2p yeast prion protein; EM, electron microscopy; FMOC, 9-fluorenylmethoxycarbonyl; TFA, trifluoroacetic acid; AFM, atomic force microscopy; MAS, magic-angle spinning; fpRFDR-CT, constant-time finite-pulse radio frequency-driven recoupling; REDOR, rotational echo double resonance; DSQ, double single-quantum; TPPM, two-pulse phase modulation; CSA, chemical shift anisotropy; MD, molecular dynamics.

10.1021/bi050724t
Published on Web 07/15/2005

fibrils have been reported (*60*). However, direct experimental evidence for side chain hydrogen bonds among glutamine or asparagine residues in amyloid fibrils has not been presented previously.

In this paper, we report the results of solid-state NMR measurements on amyloid fibrils formed by the peptide Ure2p$_{10-39}$, which represents residues 10−39 of the 354-residue Ure2p prion protein of *Saccharomyces cerevisiae*. Aggregation of Ure2p into amyloid fibrils is responsible for the self-propagating [URE3] phenotype in *S. cerevisiae* (*47*, *61*, *62*), in which the ability of the cells to stop utilization of ureidosuccinate for pyrimidine biosynthesis in the presence of ammonia is suppressed (*63*). Residues 97−354 of Ure2p form a globular domain with a glutathione *S*-transferase fold (*64*). Residues 1−80 or shorter segments thereof constitute the "prion domain" of Ure2p, which is responsible for aggregation of the full-length protein (*47*) and capable of forming amyloid fibrils that can seed fibrillization of the full-length protein (*65*, *66*). Ure2p$_{10-39}$ is the most highly conserved segment in the prion domain of Ure2p and spans the portion of the prion domain that has been shown to interfere with normal Ure2p activity when coexpressed with full-length Ure2p (*49*). Electron microscopy (EM), electron diffraction, and X-ray diffraction measurements have shown that synthetic Ure2p$_{10-39}$ forms fibrils with the morphology and cross-β structure characteristic of amyloid (*67*, *68*).

With the amino acid sequence SNLSNALRQV NIGNRNSNTT TDQSNINFEF, Ure2p$_{10-39}$ contains no hydrophobic segments longer than two residues and contains 33% glutamine and asparagine residues. The data reported below demonstrate that Ure2p$_{10-39}$ fibrils contain in-register parallel (not antiparallel) β-sheets and provide direct evidence for polar zipper interactions involving side chain amide groups of Gln18 in Ure2p$_{10-39}$ fibrils. These are the first constraints from solid-state NMR on the molecular structure of amyloid fibrils formed by a peptide that both lacks a hydrophobic segment and contains a high percentage of glutamine and asparagine residues. In addition, we present NMR data that argue against recent proposals that amyloid fibrils formed by glutamine- and asparagine-rich peptides are water-filled, tubular structures (*55*, *69*). Finally, we present two structural models for Ure2p$_{10-39}$ fibrils that are consistent with available constraints but differ in certain respects from a recent model proposed by Kajava et al. (*67*)

MATERIALS AND METHODS

Sample Preparation and Characterization. Ure2p$_{10-39}$ samples were synthesized on an Applied Biosystems 433A peptide synthesizer, using a Wang resin (0.59 mequiv/g substitution level; Anaspec, Inc.), 9-fluorenylmethoxycarbonyl (FMOC) chemistry with 2-(1*H*-benzotriazol-1-yl)-1,1,3,3-tetramethyluronium hexafluorophosphate activation, and acetic anhydride capping after each coupling step (except for the coupling of Ser10, producing a free amino terminus). The synthesis scale was 0.1 mmol, with a 10-fold excess and a 20 min coupling time for each unlabeled amino acid and a 3-fold excess and a 45 min coupling time for each labeled amino acid. Two samples were prepared for solid-state NMR, one with ^{13}C labels at the methyl carbon of Ala15, the α-carbon of Gly22, and the carbonyl carbon of Phe37 (Ure2p$_{10-39}$-AGF) and the other with a ^{13}C label at the methyl carbon of Ala15 and with uniform ^{15}N and ^{13}C labeling of Gln18 (Ure2p$_{10-39}$-AQ). Labeled FMOC amino acids were obtained from Cambridge Isotope Laboratories and Isotec. FMOC and trityl side chain protecting groups were attached to labeled L-glutamine according to published methods (*70*). Crude Ure2p$_{10-39}$ was cleaved from the synthesis resin using standard protocols [reaction for 100 min in 95% trifluoroacetic acid (TFA) with phenol, ethanedithiol, and thioanisole scavengers], precipitated in *tert*-butyl methyl ether, and dried. The crude material was purified by high-performance liquid chromatography, using a water/acetonitrile gradient with 0.1% TFA and a preparative scale Vydac C4 reverse-phase column. Samples were dissolved in TFA and then diluted with a 50% TFA/47.5% water/2.5% acetonitrile mixture before being injected onto the column. Fractions containing Ure2p$_{10-39}$ were frozen in liquid nitrogen immediately after being collected and subsequently lyophilized. Peptide purity was at least 95% as determined by electrospray mass spectrometry. The yield of purified peptide, relative to the 0.1 mmol synthesis scale, was approximately 50%.

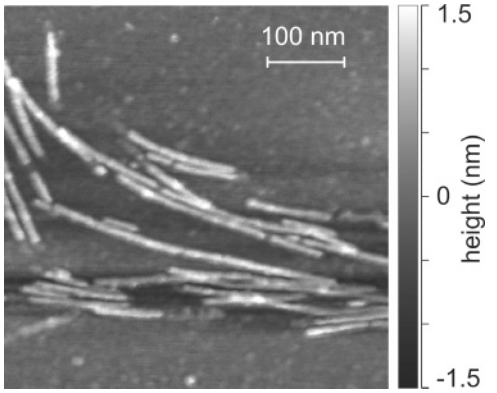

FIGURE 1: Atomic force microscope image of Ure2p$_{10-39}$ fibrils, deposited on mica and recorded in air in tapping mode.

Amyloid fibrils were formed by dissolution of purified Ure2p$_{10-39}$ at a peptide concentration of 50 μM in 10 mM phosphate buffer (pH 7.4). Dissolution was assisted by sonication. Fibrils formed immediately, appearing as a visible precipitate.

For atomic force microscopy (AFM), a 50 μL aliquot of the fibrillized solution was acidified to pH 4 by addition of 10 μL of 1% acetic acid, to promote adhesion of fibrils to the mica substrate. Approximately 10 μL of the solution was adsorbed on freshly cleaved mica for 5 min. The excess solution was then poured off, and the surface was dried in a gentle air stream. Images were obtained in air with a MultiMode AFM system (Veeco Instruments) in tapping mode, using etched silicon tips (Veeco RTESP probes, 10 nm nominal radius of curvature).

Solid-State NMR Measurements. For solid-state NMR measurements, fibrillized solutions were lyophilized and packed into 3.2 mm magic-angle spinning (MAS) rotors. Sample quantities were 3−5 mg. Measurements were performed at room temperature in Varian MAS probes operating in double-resonance ^{1}H/^{13}C or triple-resonance ^{1}H/^{13}C/^{15}N configurations, using Varian InfinityPlus-400 and Infinity-600 spectrometers. ^{13}C and ^{15}N NMR chemical shift values in Figure 2 and the discussion below are relative to tetramethylsilane and liquid NH_3, respectively. Measurements

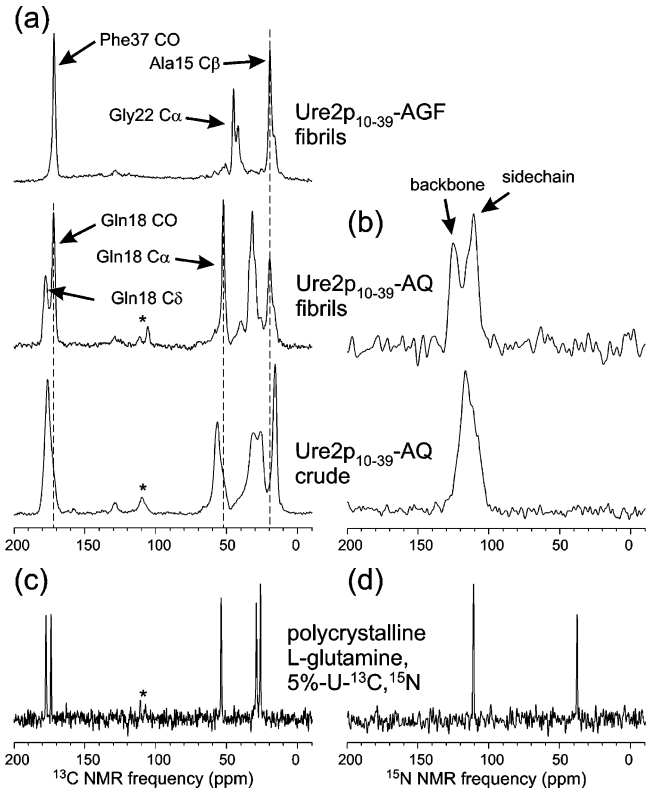

FIGURE 2: (a) Solid-state ^{13}C NMR spectra of Ure2p$_{10-39}$ in fibrillar and nonfibrillar (crude) form. The peptide is labeled with ^{13}C at the carbonyl carbon of Phe37, the α-carbon of Gly22, and the β-carbon of Ala15 (AGF) or labeled with ^{13}C at the β-carbon of Gly22 and uniformly labeled with ^{15}N and ^{13}C at Gln18 (AQ). (b) Solid-state ^{15}N NMR spectra of Ure2p$_{10-39}$-AQ. (c and d) Solid-state ^{13}C and ^{15}N NMR spectra of polycrystalline L-glutamine, in which 5% of the molecules are uniformly labeled with ^{13}C and ^{15}N. All spectra are recorded with cross-polarization, magic-angle spinning, and proton decoupling. Asterisks indicate spinning sidebands. Signals near 130 ppm in ^{13}C NMR spectra are probe background signals.

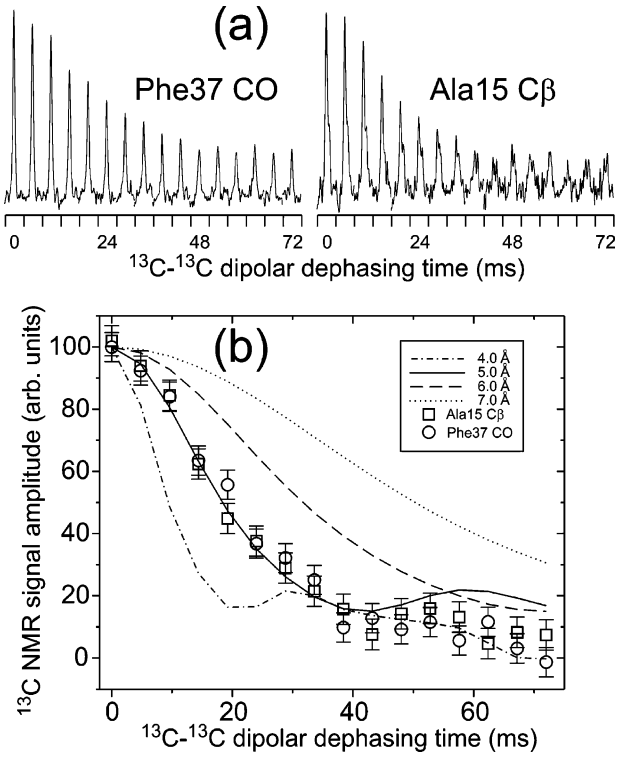

FIGURE 3: (a) Measurements of intermolecular ^{13}C−^{13}C dipole−dipole couplings in Ure2p$_{10-39}$-AGF fibrils, using the fpRFDR-CT solid-state NMR technique. Each Phe37 carbonyl or Ala15 β-carbon NMR peak is plotted in a 2.0 kHz spectral window. Peaks for dephasing times between 0 and 72 ms are concatenated to show the dipolar dephasing curves. (b) Comparison of experimental and simulated fpRFDR-CT curves, with intermolecular ^{13}C−^{13}C distances between 4.0 and 7.0 Å in the simulations. Error bars represent the root-mean-square noise in the experimental spectra. Intermolecular distances are determined to be 5.0 ± 0.3 Å for both the Phe37 carbonyl and the Ala15 β-carbon, consistent with an in-register parallel β-sheet structure in the fibrils.

of intermolecular ^{13}C−^{13}C nuclear magnetic dipole−dipole couplings were carried out on the Ure2p$_{10-39}$-AGF sample at a ^{13}C NMR frequency of 100.4 MHz and an MAS frequency of 20.0 kHz, using the constant-time, finite-pulse radio frequency-driven recoupling (fpRFDR-CT) technique (*13*, *71*). Pulse sequence conditions for fpRFDR-CT measurements were identical to those in earlier studies of Aβ fibrils (*13*, *30*).

Intermolecular distances between Ala15 methyls and between Phe37 carbonyls could be measured separately in a single sample because of the 15.3 kHz difference in ^{13}C NMR frequencies. The total experiment time for each fpRFDR-CT data set in Figure 3 was 20 h, using a pulse sequence recycle delay of 2.5 s. Measurements of intermolecular distances between Gly22 α-carbons in this sample were unsuccessful due to the relatively short transverse spin relaxation time for Gly22 α-carbons (approximately 15 ms under the conditions of fpRFDR-CT measurements), which led to a very low signal-to-noise ratio.

Intermolecular interactions among Gln18 side chain amide groups were measured in the Ure2p$_{10-39}$-AQ sample, using a newly devised solid-state NMR technique represented by the radio frequency (rf) pulse sequences in Figure 4a. This technique is an extension of the well-established rotational echo double-resonance (REDOR) (*72*) and frequency-selective REDOR (*73*) techniques for measuring ^{15}N−^{13}C dipole−dipole couplings in noncrystalline solid materials. The new technique permits the measurement of relatively weak intermolecular ^{15}N−^{13}C dipole−dipole couplings between Gln18 side chains (an approximately 3.4−5.0 Å nearest-neighbor ^{15}N−^{13}C distance in an in-register parallel β-sheet, corresponding to a 25−78 Hz coupling constant) in the presence of stronger intraresidue ^{15}N−^{13}C dipole−dipole couplings [1.338 Å chemical bond distance (*74*), corresponding to a 1280 Hz coupling constant]. In Figure 4a, a short frequency-selective REDOR pulse train (*72*, *73*) is applied during the pulse sequence period τ_1 to prepare intraresidue, heteronuclear "double single-quantum" (DSQ) coherences between directly bonded ^{13}C/^{15}N pairs in side chain amide groups. DSQ coherences are represented by spin density operator terms of the form I_xS_x in the standard product operator formalism (*75*). The intraresidue DSQ coherences are unaffected by intraresidue ^{15}N−^{13}C couplings during the longer frequency-selective REDOR dephasing period τ_d, but can decay due to intermolecular ^{15}N−^{13}C couplings if such couplings are present (because I_xS_x commutes with the effective intraresidue coupling $d_{IS}I_zS_z$ but does not commute with the effective interresidue couplings $d_{JS}J_zS_z$, where d_{IS} and d_{JS} are the effective coupling constants and J_z is the z-component of spin angular momentum for a third spin). DSQ coherences at the end of τ_d are converted to observable

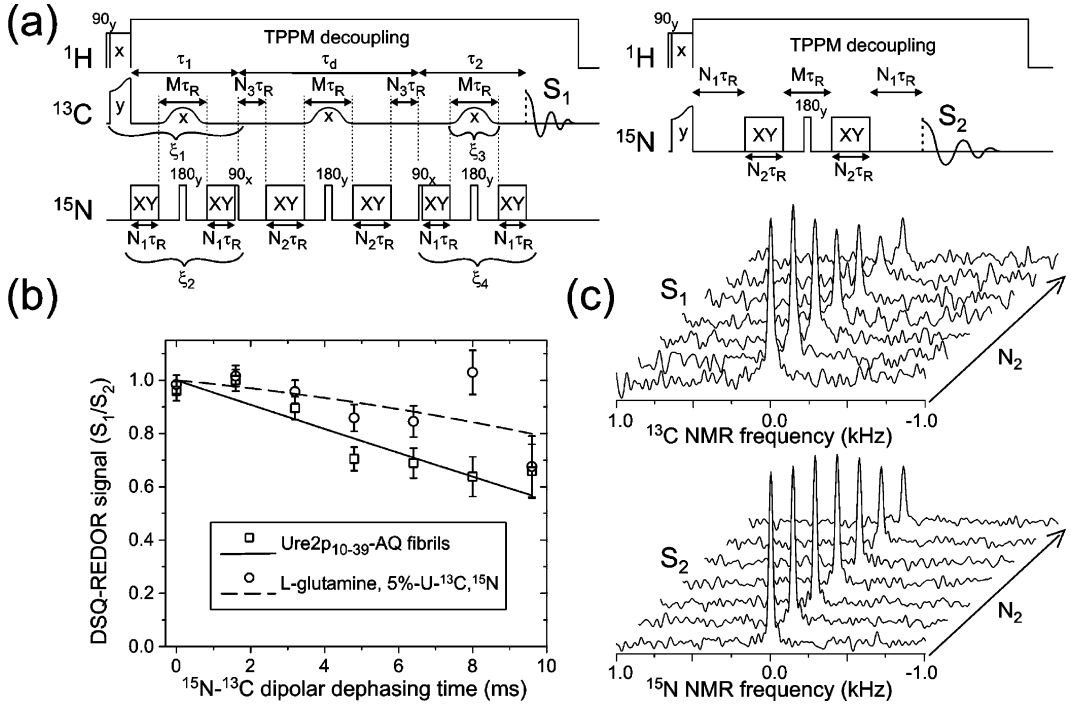

FIGURE 4: (a) Radio frequency pulse sequences for measurements of S_1 and S_2 in DSQ-REDOR experiments. The magic-angle spinning period τ_R is 100 μs. XY represents a train of ^{15}N π pulses with XY-16 phase patterns (*76*). TPPM represents two-pulse phase modulation (*77*). In these experiments, $M = N_1 = 4$, $N_2 + N_3 = 48$, and N_2 is incremented from 0 to 48 to produce effective dephasing times from 0 to 9.6 ms. Signals arising from intraresidue ^{15}N$-^{13}$C double single-quantum (DSQ) coherence are selected by phase cycling: $\xi_1 = 0, \pi, 0, \pi, 0, \pi, 0, \pi, 0, \pi, 0, \pi, 0, \pi, 0, \pi$, $\xi_2 = 0, 0, \pi, \pi, 0, 0, \pi, \pi, 0, 0, \pi, \pi, 0, 0, \pi, \pi$, $\xi_3 = 0, 0, 0, 0, \pi, \pi, \pi, \pi, 0, 0, 0, 0, \pi, \pi, \pi, \pi$, and $\xi_4 = 0, 0, 0, 0, 0, 0, 0, 0, \pi, \pi, \pi, \pi, \pi, \pi, \pi, \pi$. Signals are coadded according to the pattern $+, -, -, +, +, -, -, +, -, +, +, -, -, +, +, -$. (b) Measurements of intermolecular ^{15}N$-^{13}$C dipole−dipole couplings for glutamine side chain amide groups in Ure2p$_{10-39}$-AQ fibrils (□) and in polycrystalline [5%-U-^{13}C,^{15}N]Gln (○), using the DSQ-REDOR solid-state NMR technique. To correct for NMR signal decay due to rf pulse imperfections and nuclear spin relaxation, DSQ-REDOR points were obtained by dividing ^{13}C NMR signal amplitudes from a constant-time DSQ-REDOR measurement (S_1) by ^{15}N NMR signal amplitudes (S_2). The vertical scale is therefore in arbitrary units. Solid and dashed lines are least-squares fits to second-order polynomial functions. Error bars represent uncertainties derived from the root-mean-square noise in the experimental spectra. (c) Experimental S_1 and S_2 spectra from which the DSQ-REDOR data for Ure2p$_{10-39}$-AQ fibrils were obtained.

carbonyl ^{13}C nuclear spin polarization by the final frequency-selective REDOR pulse train during period τ_2. ^{13}C NMR signals that arise from the DSQ coherences are selected by appropriate phase cycling of rf pulses in τ_1 and τ_2. We refer to the technique depicted in Figure 4a by the acronym DSQ-REDOR.

The DSQ-REDOR measurements reported below were carried out at a ^{13}C NMR frequency of 150.65 MHz and an MAS frequency of 10.0 kHz, using 10.0 μs ^{15}N π pulses with XY-16 phase patterns (*76*), 400 μs Gaussian-shaped ^{13}C π pulses at the carbonyl ^{13}C NMR frequency (i.e., $M = 4$), and 110 kHz proton decoupling fields with two-pulse phase modulation (TPPM) (*77*) in the frequency-selective REDOR periods. Pulsed spin-lock detection (not depicted in Figure 4a) was used to enhance sensitivity (*78*). The τ_1 and τ_2 periods were 1.2 ms (i.e., $N_1 = 4$), chosen to maximize signal amplitudes. The τ_d period was fixed at 10.0 ms (i.e., $N_2 + N_3 = 48$), and N_2 was incremented from 0 to 48 in steps of 8, producing effective ^{15}N$-^{13}$C dephasing periods from 0.0 to 9.6 ms in 1.6 ms increments. The total experiment time for DSQ-REDOR measurements on Ure2p$_{10-39}$-AQ was 52 h, with a 2.0 s pulse sequence recycle delay.

We represent the DSQ-REDOR signals by $S_1(N_2)$. Use of a fixed τ_d period eliminates decay of the DSQ-REDOR signals due to transverse ^{13}C spin relaxation. Decay of DSQ-REDOR signals due to ^{15}N rf pulse imperfections during the π pulse trains in τ_d was calibrated by directly measuring the dependence of amide ^{15}N NMR signals on N_2 under experimental conditions identical to those in the DSQ-REDOR measurements. We represent the ^{15}N signal decay by $S_2(N_2)$. Decay due to the intermolecular ^{15}N$-^{13}$C dipole−dipole couplings (i.e., the data plotted in Figure 4b) is then $S_1(N_2)/S_2(N_2)$.

To verify that experimental $S_1(N_2)/S_2(N_2)$ decays were due to intermolecular ^{15}N$-^{13}$C dipole−dipole couplings as intended, rather than being due to intramolecular couplings, spin relaxation effects, or pulse sequence imperfections, we recorded DSQ-REDOR data for a 5 mg sample of polycrystalline L-glutamine in which uniformly ^{15}N- and ^{13}C-labeled molecules were diluted to 5% in unlabeled molecules by recrystallization from aqueous solution ([5%-U-^{13}C,^{15}N]Gln). Data for polycrystalline [5%-U-^{13}C,^{15}N]Gln are shown in Figures 2 and 4.

Solid-State NMR Data Analyses. Data were analyzed by comparison with numerical simulations. Simulations of fpRFDR-CT data were carried out as described previously (*13*, *30*), using a linear chain of six equally spaced ^{13}C nuclei and with initial ^{13}C spin polarization on the central two spins. Experimental fpRFDR-CT data in Figure 3 were corrected for signal contributions from natural-abundance ^{13}C nuclei by subtraction of a constant value equal to 25% (Phe37 carbonyl data) or 10% (Ala15 methyl data) of the signal at a zero effective dephasing time (*13*, *30*). Simulations of DSQ-REDOR data were carried out with a C++ program running

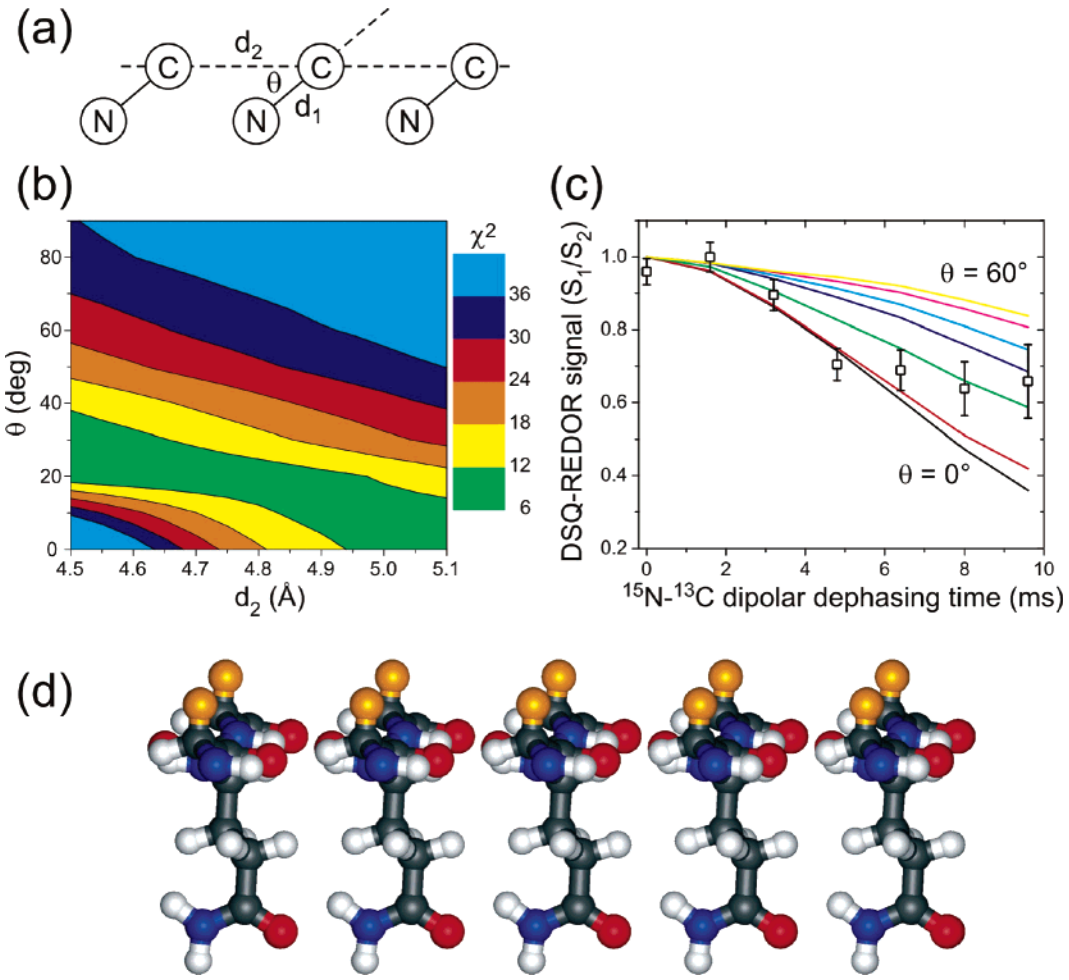

FIGURE 5: (a) Geometry of isotopically labeled glutamine side chain amide groups in DSQ-REDOR simulations. Simulations assume a ^{15}N−^{13}C amide bond length d_1 of 1.338 Å, a variable intermolecular distance d_2, and a variable angle θ. (b) Contour plot of the χ^2 deviation between experimental DSQ-REDOR data for Ure2p$_{10-39}$-AQ fibrils and simulated DSQ-REDOR data as a function of the values of d_2 and θ in the simulations. Good fits correspond to a χ^2 of ≤10. (c) Comparison of experimental and simulated DSQ-REDOR curves for a d_2 of 4.80 Å. θ varies from 0° (black line) to 60° (yellow line). (d) Molecular model for glutamine side chains pendent from an in-register parallel β-sheet in an amyloid fibril, with $\theta = 25°$. Orange atoms are β-carbons of residues that immediately precede and follow the glutamine residue in each β-strand, showing that these β-carbons are on the opposite face of the β-sheet. The spacing between β-strands is 4.80 Å. This geometry permits polar zipper interactions among glutamine side chains, as proposed by Perutz (*43*, *53*−*56*) [model generated in MOLMOL (*80*)].

under Matlab. A four-spin system (central ^{15}N−^{13}C pair plus the nearest ^{15}N and ^{13}C of flanking pairs) with the geometry shown in Figure 5a was used, with initial spin polarization on only the central ^{13}C nucleus. Six-spin simulations (all spins in Figure 5a) gave nearly identical results in test simulations, but would have required prohibitively long times to generate the contour plot in Figure 5b. DSQ-REDOR simulations included finite rf pulses, homonuclear and heteronuclear dipole−dipole couplings, ^{13}C chemical shift anisotropies (CSA), and powder averaging over 2048 orientations. CSA tensor principal values and orientations relative to chemical bonds were taken from studies of model compounds (*79*).

Molecular Modeling. Ure2p$_{10-39}$ peptides with strand−loop−strand conformations were created in MOLMOL (*80*) by assigning backbone torsion angles ϕ and ψ of −140° and 140°, respectively, to all residues and then changing these angles to 50° and 50° for Gly22 and −70° and 50° for Ser26, respectively (for the model in Figure 8a) or to −115° and 35° for Gly22 and Ser26 and −110° and −155° for Asn23 and Asn27, respectively (for the model in Figure 8b). Five copies of each peptide were combined, with 4.8 Å displacements along the intermolecular hydrogen bonding direction, to generate the starting structures for molecular dynamics (MD) and energy minimization simulations.

MD and energy minimization simulations were carried out in TINKER, version 4.2, using the CHARMM27 force field and the Force Field Explorer interface on a notebook computer. All electrostatic interactions were turned off throughout these simulations. Backbone torsion angles of residues 10−21 and 27−38 were restrained to ϕ and ψ values of −140° and 140°, respectively. Intermolecular backbone hydrogen bonds for these residues were enforced by 2.15 Å distance restraints between the appropriate carbonyl oxygens and amide protons. All other torsion angles were unrestrained. Intermolecular side chain hydrogen bonds for Gln18 and Gln33 were also enforced by distance restraints. Close contacts between β-sheets formed by residues 10−21 and 27−38 were enforced by 9.0−11.0 Å distance restraints between α-carbons of residues 12, 14, 16, and 18 and α-carbons of residues 35, 33, 31, and 29, respectively. For the model in Figure 8a, salt bridges between the side chain carboxylate group of Glu38 and the N-terminal amino group were enforced by 3.0 Å distance restraints between carboxy-

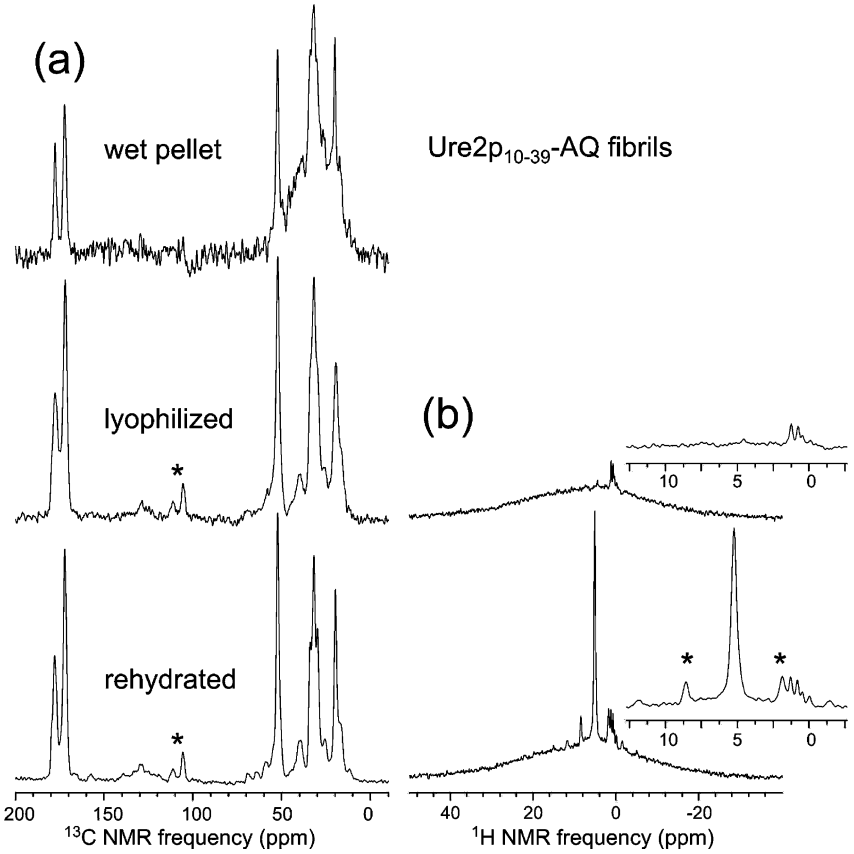

FIGURE 6: (a) ^{13}C solid-state NMR spectra of Ure2p$_{10-39}$-AQ fibrils in a fully hydrated state after fibril formation (wet pellet), after lyophilization, and after rehydration. Minor changes in ^{13}C NMR line widths, but no changes in ^{13}C NMR chemical shifts, are observed. The signal-to-noise ratio for the wet pellet is lower and the background signal (hump centered at 30 ppm) higher because of the smaller amount of sample. (b) Proton NMR spectra of the lyophilized and rehydrated samples, indicating the absence of detectable mobile water (sharp peak at 5 ppm) in the lyophilized state. Asterisks indicate spinning sidebands.

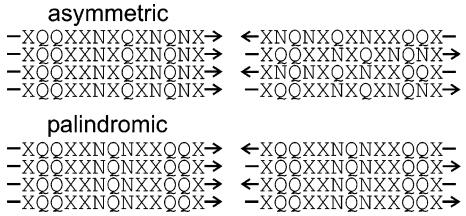

FIGURE 7: Proposal regarding the preference for in-register parallel (left) or antiparallel (right) β-sheets in amyloid fibrils formed by peptides with glutamine- and asparagine-rich sequences. Sequences with asymmetric distributions of glutamine and asparagine residues (such as Ure2p$_{10-39}$) can maximize their polar zipper interactions only in an in-register parallel β-sheet, making this the preferred structure. Sequences with palindromic distributions of glutamine and asparagine residues can maximize their polar zipper interactions in either type of β-sheet, allowing electrostatic or other interactions to determine the preferred structure.

late oxygens and amino nitrogens. For the model in Figure 8b, salt bridges between the side chain carboxylate group of Glu31 and the side chain guanidino group of Arg17 were enforced by 4.0−6.0 Å distance restraints between carboxylate carbons and guanidino carbons. Models in Figure 8 result from energy minimization of the starting structures, followed by a 10 ps MD simulation at 400 K, followed by a final energy minimization.

RESULTS

Atomic Force Microscopy Indicates that Ure2p$_{10-39}$ Aggregates Are Amyloid Fibrils. Figure 1 shows a typical AFM image of Ure2p$_{10-39}$ fibrils, obtained in air on a mica substrate. The fibrils have the characteristic straight, unbranched appearance of amyloid fibrils. In this and multiple other images, a uniform fibril height of 1.6 ± 0.1 nm was observed. Apparent fibril diameters were 12 ± 2 nm, limited by the AFM tip sharpness. In an earlier electron microscope (EM) study of Ure2p$_{10-39}$ fibrils (*67*), the fibrils appeared as 10−50 nm wide bundles of finer protofilaments, with protofilament diameters of approximately ≤5 nm. The difference between the fibril height in our AFM images and the apparent protofilament diameter in the earlier EM images may reflect an approximate 3:1 ratio of lateral dimensions (see Figure 8), with fibrils adsorbing to mica on the 5 nm faces.

X-ray diffraction data on unaligned Ure2p$_{10-39}$ fibrils obtained by Baxa et al. show the sharp 4.75 Å and broad 10 Å reflections characteristic of β-sheets in amyloid fibrils (*68*). Electron diffraction data on partially aligned Ure2p$_{10-39}$ fibrils establish the cross-β orientation of the β-sheets relative to the long axis of the fibrils that is a defining feature of amyloid fibrils (*68*).

Solid-State NMR Spectra Support an Ordered β-Sheet Structure in Ure2p$_{10-39}$ Fibrils. Panels a and b of Figure 2 show solid-state ^{13}C and ^{15}N NMR spectra of Ure2p$_{10-39}$-AGF and Ure2p$_{10-}$39-AQ fibrils in lyophilized form, as well as spectra of crude Ure2p$_{10-39}$-AQ (ether precipitate after cleavage from the synthesis resin and drying, with no purification or fibrillization). The similarity of Ala15 methyl signals in ^{13}C NMR spectra of Ure2p$_{10-39}$-AGF and

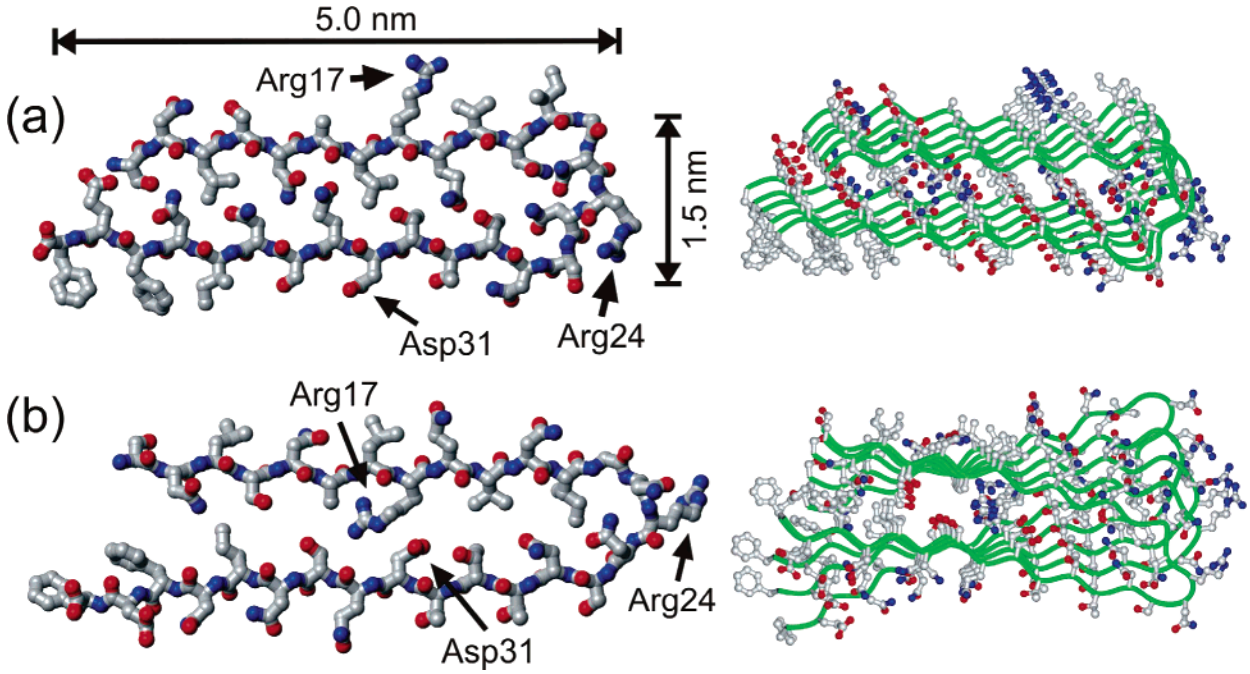

FIGURE 8: Structural models for Ure2p$_{10-39}$ fibrils generated by restrained molecular dynamics and energy minimization simulations for a pentameric assembly of Ure2p$_{10-39}$ molecules. Both the final energy-minimized structure of the pentamer (right) and the conformation of the central molecule in the pentamer (left) are shown. The two models differ in the relative orientation of the β-sheets formed by the two β-strand segments (residues 10−21 and 27−39), as dictated by the conformation of the intervening loop segment (residues 22−26). (a) Model in which all charged side chains are outside the fibril core. (b) Model in which oppositely charged side chains of Arg17 and Asp31 can form internal salt bridges in the fibril core.

Ure2p$_{10-39}$-AQ fibrils demonstrates the reproducibility of the fibril structures. Line widths in ^{13}C NMR spectra of fibrillized Ure2p$_{10-39}$-AQ (2.0−2.9 ppm full width at half-maximum) are shorter than in spectra of crude Ure2p$_{10-39}$-AQ (3.0−5.1 ppm), indicating a higher degree of structural order in the fibrils. The development of resolved ^{13}C and ^{15}N NMR signals for the Gln18 side chain carbonyl carbon and amide nitrogen upon fibril formation indicates that Gln18 side chains are well-ordered. In the fibrils, ^{13}C chemical shifts for carbonyl sites of Gln18 and Phe37 (171.9 and 171.6 ppm), the α-carbon of Gln18 (52.3 ppm), and the β-carbon of Ala15 (19.4 ppm) exhibit deviations from random coil values [174.3, 174.1, 54.0, and 17.4 ppm, respectively (*81*)] that are consistent in both sign and magnitude with β-strand backbone conformations at these residues [i.e., upfield shift for carbonyls and α-carbons, downfield shift for β-carbons (*6*, *82*−*84*)]. The α-carbon signal for Gly22 is split into two components (45.2 and 42.1 ppm, vs a random coil value of 43.4 ppm), suggesting the coexistence of two backbone conformations at Gly22 in Ure2p$_{10-39}$ fibrils, at least one of which may be a non-β-strand conformation. Similar splittings of ^{13}C NMR lines have been observed for certain residues in the non-β-strand segment of Aβ fibrils (*30*). The conformational interpretation of α-carbon chemical shifts for glycine residues is generally more ambiguous than for other residues, as the range of secondary shifts for glycines in proteins is relatively small and does not show a clear separation of values corresponding to helical and extended backbone conformations.

In crude Ure2p$_{10-39}$-AQ, ^{13}C chemical shifts for the carbonyl and α-carbon of Gln18 (176.4 and 56.8 ppm) and the β-carbon of Ala15 (15.9 ppm) are consistent with α-helical conformations at these residues. Thus, the peptide conformations in ether-precipitated and fibrillized forms are substantially different, as previously observed for Aβ fibrils (*7*).

The assignment of ^{15}N NMR lines to side chain and backbone amide sites indicated in Figure 2 was determined from ^{13}C-detected frequency-selective REDOR measurements (*73*), in which selective excitation of the ^{15}N NMR line at 111 ppm produced greater dephasing of the Gln18 δ-carbon and selective excitation of the ^{15}N NMR line at 125 ppm produced greater dephasing of the Gln18 α-carbon. The measurements were performed with MAS at 9.00 kHz, Gaussian-shaped selective pulses with 1.111 ms durations, and 1.78 ms dephasing periods.

Panels c and d of Figure 2 show solid-state NMR spectra of polycrystalline [5%-U-^{13}C,^{15}N]Gln. Line widths in these spectra are less than 0.8 ppm, as expected for a polycrystalline material. Line widths for Ure2p$_{10-39}$ fibrils are typical of conformationally ordered peptides in rigid, noncrystalline environments (*16*, *30*, *85*−*87*).

Intermolecular ^{13}C−^{13}C Dipole−Dipole Couplings Indicate Parallel β-Sheets. Figure 3 shows measurements of intermolecular ^{13}C−^{13}C nuclear magnetic dipole−dipole couplings for Ure2p$_{10-39}$-AGF fibrils, using the fpRFDR-CT technique as in earlier studies of Aβ fibrils (*13*, *30*). The time scale for decay of ^{13}C NMR signals in fpRFDR-CT measurements decreases with a decreasing distance between ^{13}C labels on neighboring peptide molecules, due to the $1/R^3$ dependence of dipole−dipole coupling strengths on internuclear distance R. Intermolecular distances for Ala15 methyl labels and Phe37 carbonyl labels were measured separately by positioning the rf carrier frequency in the fpRFDR-CT pulse sequence at either 32.2 ppm (Ala15 methyl data) or 162.1 ppm (Phe37 carbonyl data). The time scale for signal decay was approximately 30 ms in both measurements. Comparison with numerical simulations (Figure 3b) indicates

intermolecular distances of 5.0 ± 0.3 Å for both Ala15 methyl labels and Phe37 carbonyl labels. This result is consistent with an in-register parallel β-sheet structure in Ure2p$_{10-39}$ fibrils, as previously observed for fibrils formed by the 40-residue and 42-residue variants of full-length Aβ and fibrils formed by residues 10−35 of Aβ (*12*, *13*, *30*). In an ideal in-register parallel β-sheet, the intermolecular distances would be 4.7−4.8 Å.

Computer modeling of parallel β-sheets with a one-residue shift from in-register alignment of neighboring peptide chains shows that nearest-neighbor intermolecular distances would be approximately 5.2 Å for backbone carbonyl labels and approximately 6.7 Å for alanine methyl labels. Thus, the data in Figure 3 for Ala15 rule out a one-residue (or greater) shift. Data in Figure 3 are also inconsistent with an antiparallel β-sheet structure, which could not produce the observed 5.0 ± 0.3 Å intermolecular distances for both Ala15 and Phe37 simultaneously.

Intermolecular ^{15}N−^{13}C Dipole−Dipole Couplings Indicate Gln18 Side Chain Interactions. Figure 4b shows measurements of intermolecular ^{15}N−^{13}C nuclear magnetic dipole−dipole couplings among side chain amide groups of Gln18 residues in Ure2p$_{10-39}$-AQ fibrils, using the DSQ-REDOR technique shown in Figure 4a. As explained above, the DSQ-REDOR technique was designed specifically to permit measurements of intermolecular ^{15}N−^{13}C couplings in the presence of the stronger intraresidue ^{15}N−^{13}C couplings in the Ure2p$_{10-39}$-AQ sample. Intraresidue couplings are present because Gln18 is uniformly labeled with ^{15}N and ^{13}C in this sample. Data points in Figure 4b were obtained from the experimental ^{13}C and ^{15}N NMR spectra in Figure 4c. Only signals from Gln18 side chain carbonyl carbons contribute to the ^{13}C NMR spectra in Figure 4c because other carbon signals are removed by DSQ filtering (i.e., by rf phase shifts ξ_1, ξ_2, ξ_3, and ξ_4 in Figure 4a).

That the DSQ-REDOR signal decay for Ure2p$_{10-39}$-AQ fibrils is primarily due to intermolecular couplings is supported by DSQ-REDOR data for polycrystalline [5%-U-^{13}C,^{15}N]Gln, also shown in Figure 4b, which decay significantly more slowly. On the basis of the reported crystal structure of L-glutamine (*74*), an isotopically labeled side chain amide group in [5%-U-^{13}C,^{15}N]Gln has a 26% probability of being within 4.5 Å of a ^{15}N or ^{13}C site on a neighboring molecule to which it will couple under the DSQ-REDOR pulse sequence, and the intramolecular distance between side chain carbonyl ^{13}C and amine ^{15}N sites is 4.491 Å. The experimental DSQ-REDOR decay for [5%-U-^{13}C,^{15}N]Gln in Figure 4b is consistent with the crystal structure and isotopic dilution level.

The DSQ-REDOR data for Ure2p$_{10-39}$-AQ fibrils are analyzed by comparison with numerical simulations. As depicted in Figure 5a, these simulations assume a geometry for Gln18 side chain amide groups in which the intraresidue ^{15}N−^{13}C chemical bond distance d_1 is fixed at 1.338 Å (*74*), the intermolecular distance d_2 is fixed at a value between 4.50 and 5.10 Å, and the angle θ between the chemical bonds and the intermolecular displacement is allowed to vary. Note that this assumed geometry applies to all possible Gln18 side chain conformations, provided that the β-sheets are planar and the structure has translational symmetry. Deviations from planarity in the β-sheets of amyloid fibrils are expected to be small, corresponding to a twist of less than 10° per β-strand, based on the fact that fibril morphologies commonly exhibit twist periods greater than 20 nm (*2*, *5*, *12*, *14*, *15*, *30*). Approximate translational symmetry in Ure2p$_{10-39}$ fibrils is supported by the relatively sharp solid-state NMR lines for Gln18 in Figure 2. Figure 5b shows a contour plot of the χ^2 deviation between experimental and simulated DSQ-REDOR data as a function of θ and d_2. Simulated DSQ-REDOR data for a d_2 of 4.80 Å are compared with the experimental data in Figure 5c. Given that d_2 lies in the 4.65−4.85 Å range in β-sheets (based on examination of C_α−C_α distances across parallel β-sheets in high-resolution protein crystal structures, e.g., Protein Data Bank entries 1R2R and 1J8Q), we conclude that $\theta = 25 \pm 5°$. Figure 5d shows a molecular model for Gln18 side chain interactions that is consistent with the best-fit geometry. This model appears to be compatible with the polar zipper hydrogen bonds proposed by Perutz (*43*, *53*, *55*).

Effects of Hydration on Solid-State NMR Spectra Argue against a Water-Filled Structure. Perutz and co-workers also proposed that amyloid fibrils formed by glutamine- and asparagine-rich peptides might have water-filled, tubular structures (*55*). X-ray fiber diffraction data for Sup35 fibrils have been presented as support for this proposal (*69*). Figure 6a shows solid-state ^{13}C NMR spectra of Ure2p$_{10-39}$-AQ fibrils, examined as a centrifuged pellet of the initial fibrillized solution prior to lyophilization, as a dry, lyophilized powder, and as a lyophilized powder to which a small aliquot of 10 mM phosphate buffer (approximately 90 water molecules per peptide molecule) has been added. No differences in ^{13}C NMR chemical shifts are observed in these three hydration states. The increased ^{13}C NMR line widths in the dry, lyophilized state (by 0.6, 0.4, 0.4, and 2.0 ppm for Gln18 side chain carbonyl, Gln18 backbone carbonyl, Gln18 α-carbon, and Ala15 β-carbon lines, respectively) can be attributed to inhomogeneous broadening from local static structural disorder in these noncrystalline materials, e.g., minor variations in backbone and side chain torsion angles from one Ure2p$_{10-39}$ molecule to the next. In the hydrated state, librational motions and side chain dynamics can average out some of the local structural disorder, producing sharper NMR lines.

^{1}H NMR spectra in Figure 6b show that the dry, lyophilized state indeed contains no detectable, mobile water (fewer than three mobile water molecules per peptide molecule, based on the signal-to-noise ratio for the water peak in Figure 6b). Data in Figure 6 are incompatible with the possibility that fully hydrated Ure2p$_{10-39}$ fibrils have a water-filled tubular structure that undergoes a major change upon drying, such as collapse to a laminated β-sheet structure (*69*). Hydration apparently affects molecular motions, but not structure. These conclusions from solid-state NMR spectra may be related to the work of Diaz-Avalos et al., in which diffraction measurements on a seven-residue, glutamine- and asparagine-rich peptide in an amyloid-like nanocrystalline form revealed a low density of water, attributed to side chain hydrogen bonding (*88*).

Rehydration of the Ure2p$_{10-39}$-AGF fibril sample also produced no changes in the ^{13}C chemical shifts (<0.1 ppm change in peak positions). ^{13}C NMR lines for the Ph37 carbonyl and Gly22 α-carbon sites were reduced by approximately 0.5 ppm by rehydration. Similarly, ^{15}N NMR line widths for Gln18 in Ure2p$_{10-39}$-AQ fibrils were reduced

from ~8 to ~4 ppm by rehydration, but no changes in ^{15}N chemical shifts were observed.

DISCUSSION

Data presented above lead to the following conclusions. (1) Ure2p$_{10-39}$ fibrils contain well-ordered β-sheets with an in-register parallel structure. (2) Ala15, Gln18, and Phe37 are contained in β-strands that participate in the parallel β-sheets, but Gly22 may be contained in a non-β-strand segment with two alternative conformations. (3) The amide groups of Gln18 side chains exhibit intermolecular ^{15}N−^{13}C dipole−dipole couplings that are consistent with polar zipper hydrogen bond interactions. (4) The molecular structure of Ure2p$_{10-39}$ fibrils is not strongly dependent on hydration.

With the exception of studies of the designed peptide ccβ (*23*) and the HET-s prion protein (*35*), previous solid-state NMR studies of amyloid fibril structures have focused on peptides with hydrophobic segments, at least five residues in length (*1*, *3*−*8*, *12*, *13*, *16*, *18*, *22*, *24*, *25*, *30*, *89*, *90*). Both parallel and antiparallel β-sheet structures have been observed in these studies, but in all cases, the structures are such that hydrophobic contacts within a single β-sheet layer are maximized (*3*, *5*−*8*, *12*, *13*, *16*, *30*) or nearly maximized (*1*, *25*). Ure2p$_{10-39}$ is a qualitatively different case because of its lack of hydrophobic segments. The observation of an in-register parallel β-sheet structure (Figure 3) and the evidence for polar zipper interactions in Ure2p$_{10-39}$ fibrils (Figures 4 and 5) suggest that the parallel β-sheet structure is favored in amyloid fibrils by side chain interactions among polar groups as well as hydrophobic groups within a single β-sheet layer. In particular, an in-register parallel β-sheet structure would be favored over out-of-register or antiparallel structures when the peptide sequence contains an asymmetric distribution of glutamine and asparagine residues, as depicted in Figure 7. A sequence that is palindromic with respect to glutamine and asparagine residues could form either parallel or antiparallel β-sheets, with the choice being dictated by electrostatic or other interactions. We hypothesize that hydrogen bonds between a glutamine side chain and an asparagine side chain would not occur, because of the different side chain lengths, so a peptide containing a mixture of glutamine and asparagine residues would adopt a β-sheet structure that aligns glutamines with glutamines and asparagines with asparagines.

The recent observation by Ross et al. that scrambling of the Ure2p prion domain sequence does not suppress fibril formation (*91*) is consistent with an in-register parallel β-sheet structure stabilized by polar zipper interactions, since all polar zipper interactions could be present in such a structure with any ordering of the amino acids. In contrast, a rearrangement of the amino acid sequence of residues 10−35 of Aβ that eliminates the central hydrophobic segment of this peptide, but preserves the amino acid composition, has been shown to suppress both fibril formation and parallel β-sheet formation (*12*). Thus, amyloid fibril formation that is dependent on amino acid composition but independent of sequence order may be a unique property of glutamine- and asparagine-rich peptides.

Although both hydrophobic interactions and polar zipper interactions appear to favor an in-register parallel β-sheet structure for a generic amyloid-forming peptide with an asymmetric distribution of hydrophobic segments or glutamine and asparagine residues, such a structure could be destabilized by electrostatic repulsions between charged side chains of neighboring peptide molecules if the charges were located in the low-dielectric core of the fibril. As exemplified by recent molecular structural models for full-length Aβ fibrils (*16*, *30*, *31*, *92*, *93*), electrostatic destabilization of an in-register parallel β-sheet structure can be avoided by adoption of a peptide conformation that places charges on the exterior of the fibril structure, where charged groups can be fully solvated, and by pairing of oppositely charged side chains in the interior of the fibril structure. Figure 8 shows two specific models for the structure of Ure2p$_{10-39}$ fibrils, generated by restrained MD and energy minimization simulations (see Materials and Methods). These models are consistent with the solid-state NMR data presented above and prevent electrostatic destabilization either by placing side chains of Arg17, Arg24, Asp32, and Glu38 outside the fibril core (Figure 8a) or by placing side chains of Arg24 and Glu38 outside the fibril core and pairing side chains of Arg17 with those of Asp31 (Figure 8b). In these models, Ure2p$_{10-39}$ adopts a strand−loop−strand conformation similar to the peptide conformation in the Aβ fibril model of Petkova et al. (*16*, *30*, *31*). The loop segment begins at Gly22, consistent with the solid-state ^{13}C NMR chemical shifts for this residue discussed above, and ends before the three threonines in the Ure2p$_{10-39}$ sequence, consistent with the stabilization of β-strands in globular proteins by threonine residues (*94*, *95*). The approximate 1.5 nm fibril "height" in these models is consistent with our AFM data (Figure 1) if the β-sheets are untwisted, while the approximate 5 nm fibril "width" may be consistent with the EM images reported by Kajava et al. (*67*). Interestingly, the model in Figure 8a remains untwisted in the course of MD and energy minimization simulations, while the model in Figure 8b develops a twist of roughly 8° per β-strand about the long axis of the fibril. Twisting of the model in Figure 8b appears to result from strain due to the presence of the bulky Phe37 side chain in the fibril core and the relatively tight loop conformation adopted by residues 22−26.

The models in Figure 8 differ from the "β-serpentine" model for Ure2p$_{10-39}$ fibrils proposed recently by Kajava et al. (*67*) (which was based in part on the data in Figure 3) in that the models in Figure 8 contain two, rather than four, β-strand segments, place Gly22 in the loop, rather than in a β-strand, and (for the model in Figure 8b) contain charged side chains in the core. Additional experimental constraints are required to confirm any of these models or to provide directions for their refinement.

Finally, Thakur and Wetzel have shown that the effects on aggregation kinetics and fibril formation of the introduction of Pro-Gly pairs into long polyglutamine chains are sensitive to the spacing between Pro-Gly pairs, with strong effects when Pro-Gly pairs are separated by fewer than nine glutamine residues (*60*). This result suggests that the β-strands in polyglutamine fibrils are at least eight residues in length. Although Thakur and Wetzel interpret their data in terms of an antiparallel β-sheet structure (*60*), their data may also be consistent with structures analogous to the models in Figure 8. For polyglutamine peptides of the type studied by Thakur and Wetzel, most polar zipper interactions

could be present in either antiparallel or parallel β-sheet structures. Other interactions may then dictate the β-sheet structures that actually form in their experiments.

ACKNOWLEDGMENT

We thank Drs. R. B. Wickner and U. Baxa for useful discussions throughout the course of this work.

REFERENCES

1. Lansbury, P. T., Costa, P. R., Griffiths, J. M., Simon, E. J., Auger, M., Halverson, K. J., Kocisko, D. A., Hendsch, Z. S., Ashburn, T. T., Spencer, R. G. S., Tidor, B., and Griffin, R. G. (1995) Structural model for the β-amyloid fibril based on interstrand alignment of an antiparallel-sheet comprising a C-terminal peptide, *Nat. Struct. Biol. 2*, 990−998.
2. Sunde, M., Serpell, L. C., Bartlam, M., Fraser, P. E., Pepys, M. B., and Blake, C. C. F. (1997) Common core structure of amyloid fibrils by synchrotron X-ray diffraction, *J. Mol. Biol. 273*, 729−739.
3. Benzinger, T. L. S., Gregory, D. M., Burkoth, T. S., Miller-Auer, H., Lynn, D. G., Botto, R. E., and Meredith, S. C. (1998) Propagating structure of Alzheimer's β-amyloid(10−35) is parallel β-sheet with residues in exact register, *Proc. Natl. Acad. Sci. U.S.A. 95*, 13407−13412.
4. Gregory, D. M., Benzinger, T. L. S., Burkoth, T. S., Miller-Auer, H., Lynn, D. G., Meredith, S. C., and Botto, R. E. (1998) Dipolar recoupling NMR of biomolecular self-assemblies: Determining inter- and intrastrand distances in fibrilized Alzheimer's β-amyloid peptide, *Solid State Nucl. Magn. Reson. 13*, 149−166.
5. Antzutkin, O. N., Balbach, J. J., Leapman, R. D., Rizzo, N. W., Reed, J., and Tycko, R. (2000) Multiple quantum solid-state NMR indicates a parallel, not antiparallel, organization of β-sheets in Alzheimer's β-amyloid fibrils, *Proc. Natl. Acad. Sci. U.S.A. 97*, 13045−13050.
6. Balbach, J. J., Ishii, Y., Antzutkin, O. N., Leapman, R. D., Rizzo, N. W., Dyda, F., Reed, J., and Tycko, R. (2000) Amyloid fibril formation by $A\beta_{16-22}$, a seven-residue fragment of the Alzheimer's β-amyloid peptide, and structural characterization by solid-state NMR, *Biochemistry 39*, 13748−13759.
7. Benzinger, T. L. S., Gregory, D. M., Burkoth, T. S., Miller-Auer, H., Lynn, D. G., Botto, R. E., and Meredith, S. C. (2000) Two-dimensional structure of β-amyloid(10−35) fibrils, *Biochemistry 39*, 3491−3499.
8. Burkoth, T. S., Benzinger, T. L. S., Urban, V., Morgan, D. M., Gregory, D. M., Thiyagarajan, P., Botto, R. E., Meredith, S. C., and Lynn, D. G. (2000) Structure of the β-amyloid(10−35) fibril, *J. Am. Chem. Soc. 122*, 7883−7889.
9. Kheterpal, I., Zhou, S., Cook, K. D., and Wetzel, R. (2000) Aβ amyloid fibrils possess a core structure highly resistant to hydrogen exchange, *Proc. Natl. Acad. Sci. U.S.A. 97*, 13597−13601.
10. Serpell, L. C., and Smith, J. M. (2000) Direct visualisation of the β-sheet structure of synthetic Alzheimer's amyloid, *J. Mol. Biol. 299*, 225−231.
11. Kheterpal, I., Williams, A., Murphy, C., Bledsoe, B., and Wetzel, R. (2001) Structural features of the Aβ amyloid fibril elucidated by limited proteolysis, *Biochemistry 40*, 11757−11767.
12. Antzutkin, O. N., Leapman, R. D., Balbach, J. J., and Tycko, R. (2002) Supramolecular structural constraints on Alzheimer's β-amyloid fibrils from electron microscopy and solid-state nuclear magnetic resonance, *Biochemistry 41*, 15436−15450.
13. Balbach, J. J., Petkova, A. T., Oyler, N. A., Antzutkin, O. N., Gordon, D. J., Meredith, S. C., and Tycko, R. (2002) Supramolecular structure in full-length Alzheimer's β-amyloid fibrils: Evidence for a parallel β-sheet organization from solid-state nuclear magnetic resonance, *Biophys. J. 83*, 1205−1216.
14. Jimenez, J. L., Nettleton, E. J., Bouchard, M., Robinson, C. V., Dobson, C. M., and Saibil, H. R. (2002) The protofilament structure of insulin amyloid fibrils, *Proc. Natl. Acad. Sci. U.S.A. 99*, 9196−9201.
15. Jimenez, J. L., Guijarro, J. L., Orlova, E., Zurdo, J., Dobson, C. M., Sunde, M., and Saibil, H. R. (1999) Cryo-electron microscopy structure of an SH3 amyloid fibril and model of the molecular packing, *EMBO J. 18*, 815−821.
16. Petkova, A. T., Ishii, Y., Balbach, J. J., Antzutkin, O. N., Leapman, R. D., Delaglio, F., and Tycko, R. (2002) A structural model for Alzheimer's β-amyloid fibrils based on experimental constraints from solid-state NMR, *Proc. Natl. Acad. Sci. U.S.A. 99*, 16742−16747.
17. Torok, M., Milton, S., Kayed, R., Wu, P., McIntire, T., Glabe, C. G., and Langen, R. (2002) Structural and dynamic features of Alzheimer's Aβ peptide in amyloid fibrils studied by site-directed spin labeling, *J. Biol. Chem. 277*, 40810−40815.
18. Antzutkin, O. N., Balbach, J. J., and Tycko, R. (2003) Site-specific identification of non-β-strand conformations in Alzheimer's β-amyloid fibrils by solid-state NMR, *Biophys. J. 84*, 3326−3335.
19. Der-Sarkissian, A., Jao, C. C., Chen, J., and Langen, R. (2003) Structural organization of α-synuclein fibrils studied by site-directed spin labeling, *J. Biol. Chem. 278*, 37530−37535.
20. Kheterpal, I., Lashuel, H. A., Hartley, D. M., Wlaz, T., Lansbury, P. T., and Wetzel, R. (2003) Aβ protofibrils possess a stable core structure resistant to hydrogen exchange, *Biochemistry 42*, 14092−14098.
21. Gordon, D. J., Balbach, J. J., Tycko, R., and Meredith, S. C. (2004) Increasing the amphiphilicity of an amyloidogenic peptide changes the β-sheet structure in the fibrils from antiparallel to parallel, *Biophys. J. 86*, 428−434.
22. Jaroniec, C. P., MacPhee, C. E., Bajaj, V. S., McMahon, M. T., Dobson, C. M., and Griffin, R. G. (2004) High-resolution molecular structure of a peptide in an amyloid fibril determined by magic angle spinning NMR spectroscopy, *Proc. Natl. Acad. Sci. U.S.A. 101*, 711−716.
23. Kammerer, R. A., Kostrewa, D., Zurdo, J., Detken, A., Garcia-Echeverria, C., Green, J. D., Muller, S. A., Meier, B. H., Winkler, F. K., Dobson, C. M., and Steinmetz, M. O. (2004) Exploring amyloid formation by a de novo design, *Proc. Natl. Acad. Sci. U.S.A. 101*, 4435−4440.
24. Oyler, N. A., and Tycko, R. (2004) Absolute structural constraints on amyloid fibrils from solid state NMR spectroscopy of partially oriented samples, *J. Am. Chem. Soc. 126*, 4478−4479.
25. Petkova, A. T., Buntkowsky, G., Dyda, F., Leapman, R. D., Yau, W. M., and Tycko, R. (2004) Solid-state NMR reveals a pH-dependent antiparallel β-sheet registry in fibrils formed by a β-amyloid peptide, *J. Mol. Biol. 335*, 247−260.
26. Shivaprasad, S., and Wetzel, R. (2004) An intersheet packing interaction in Aβ fibrils mapped by disulfide cross-linking, *Biochemistry 43*, 15310−15317.
27. Tycko, R. (2004) Progress towards a molecular-level structural understanding of amyloid fibrils, *Curr. Opin. Struct. Biol. 14*, 96−103.
28. Williams, A. D., Portelius, E., Kheterpal, I., Guo, J. T., Cook, K. D., Xu, Y., and Wetzel, R. (2004) Mapping Aβ amyloid fibril secondary structure using scanning proline mutagenesis, *J. Mol. Biol. 335*, 833−842.
29. Makin, O. S., Atkins, E., Sikorski, P., Johansson, J., and Serpell, L. C. (2005) Molecular basis for amyloid fibril formation and stability, *Proc. Natl. Acad. Sci. U.S.A. 102*, 315−320.
30. Petkova, A. T., Leapman, R. D., Guo, Z. H., Yau, W. M., Mattson, M. P., and Tycko, R. (2005) Self-propagating, molecular-level polymorphism in Alzheimer's β-amyloid fibrils, *Science 307*, 262−265.
31. Tycko, R. (2003) Insights into the amyloid folding problem from solid-state NMR, *Biochemistry 42*, 3151−3159.
32. Naito, A., Kamihira, M., Inoue, R., and Saito, H. (2004) Structural diversity of amyloid fibril formed in human calcitonin as revealed by site-directed ^{13}C solid-state NMR spectroscopy, *Magn. Reson. Chem. 42*, 247−257.
33. Kamihira, M., Oshiro, Y., Tuzi, S., Nosaka, A. Y., Saito, H., and Naito, A. (2003) Effect of electrostatic interaction on fibril formation of human calcitonin as studied by high-resolution solid state ^{13}C NMR, *J. Biol. Chem. 278*, 2859−2865.
34. Kamihira, M., Naito, A., Tuzi, S., Nosaka, A. Y., and Saito, H. (2000) Conformational transitions and fibrillation mechanism of human calcitonin as studied by high-resolution solid state ^{13}C NMR, *Protein Sci. 9*, 867−877.
35. Siemer, A. B., Ritter, C., Ernst, M., Riek, R., and Meier, B. H. (2005) High-resolution solid-state NMR spectroscopy of the prion protein HET-s in its amyloid conformation, *Angew. Chem., Int. Ed. 44*, 2441−2444.
36. Booth, D. R., Sunde, M., Bellotti, V., Robinson, C. V., Hutchinson, W. L., Fraser, P. E., Hawkins, P. N., Dobson, C. M., Radford, S. E., Blake, C. C. F., and Pepys, M. B. (1997) Instability, unfolding and aggregation of human lysozyme variants underlying amyloid fibrillogenesis, *Nature 385*, 787−793.

37. Guijarro, J. I., Sunde, M., Jones, J. A., Campbell, I. D., and Dobson, C. M. (1998) Amyloid fibril formation by an SH3 domain, *Proc. Natl. Acad. Sci. U.S.A. 95*, 4224−4228.
38. Chiti, F., Webster, P., Taddei, N., Clark, A., Stefani, M., Ramponi, G., and Dobson, C. M. (1999) Designing conditions for in vitro formation of amyloid protofilaments and fibrils, *Proc. Natl. Acad. Sci. U.S.A. 96*, 3590−3594.
39. Pertinhez, T. A., Bouchard, M. L., Tomlinson, E. J., Wain, R., Ferguson, S. J., Dobson, C. M., and Smith, L. J. (2001) Amyloid fibril formation by a helical cytochrome, *FEBS Lett. 495*, 184−186.
40. Fandrich, M., Forge, V., Buder, K., Kittler, M., Dobson, C. M., and Diekmann, S. (2003) Myoglobin forms amyloid fibrils by association of unfolded polypeptide segments, *Proc. Natl. Acad. Sci. U.S.A. 100*, 15463−15468.
41. Dobson, C. M. (2003) Protein folding and misfolding, *Nature 426*, 884−890.
42. Jayasinghe, S. A., and Langen, R. (2004) Identifying structural features of fibrillar islet amyloid polypeptide using site-directed spin labeling, *J. Biol. Chem. 279*, 48420−48425.
43. Perutz, M. F. (1996) Glutamine repeats and inherited neurodegenerative diseases: Molecular aspects, *Curr. Opin. Struct. Biol. 6*, 848−858.
44. Macdonald, M. E., Ambrose, C. M., Duyao, M. P., Myers, R. H., Lin, C., Srinidhi, L., Barnes, G., Taylor, S. A., James, M., Groot, N., Macfarlane, H., Jenkins, B., Anderson, M. A., Wexler, N. S., Gusella, J. F., Bates, G. P., Baxendale, S., Hummerich, H., Kirby, S., North, M., Youngman, S., Mott, R., Zehetner, G., Sedlacek, Z., Poustka, A., Frischauf, A. M., Lehrach, H., Buckler, A. J., Church, D., Doucettestamm, L., Odonovan, M. C., Ribaramirez, L., Shah, M., Stanton, V. P., Strobel, S. A., Draths, K. M., Wales, J. L., Dervan, P., Housman, D. E., Altherr, M., Shiang, R., Thompson, L., Fielder, T., Wasmuth, J. J., Tagle, D., Valdes, J., Elmer, L., Allard, M., Castilla, L., Swaroop, M., Blanchard, K., Collins, F. S., Snell, R., Holloway, T., Gillespie, K., Datson, N., Shaw, D., and Harper, P. S. (1993) A novel gene containing a trinucleotide repeat that is expanded and unstable on Huntington's disease chromosomes, *Cell 72*, 971−983.
45. Bevivino, A. E., and Loll, P. J. (2001) An expanded glutamine repeat destabilizes native ataxin-3 structure and mediates parallel β-fibrils, *Proc. Natl. Acad. Sci. U.S.A. 98*, 11955−11960.
46. DePace, A. H., Santoso, A., Hillner, P., and Weissman, J. S. (1998) A critical role for amino-terminal glutamine/asparagine repeats in the formation and propagation of a yeast prion, *Cell 93*, 1241−1252.
47. Masison, D. C., and Wickner, R. B. (1995) Prion-inducing domain of yeast Ure2p and protease resistance of Ure2p prion-containing cells, *Science 270*, 93−95.
48. Santoso, A., Chien, P., Osherovich, L. Z., and Weissman, J. S. (2000) Molecular basis of a yeast prion species barrier, *Cell 100*, 277−288.
49. Edskes, H. K., and Wickner, R. B. (2002) Conservation of a portion of the *S. cerevisiae* Ure2p prion domain that interacts with the full-length protein, *Proc. Natl. Acad. Sci. U.S.A. 99*, 16384−16391.
50. Baxa, U., Taylor, K. L., Wall, J. S., Simon, M. N., Cheng, N. Q., Wickner, R. B., and Steven, A. C. (2003) Architecture of Ure2p prion filaments: The N-terminal domains form a central core fiber, *J. Biol. Chem. 278*, 43717−43727.
51. Urry, D. W. (2004) The change in Gibbs free energy for hydrophobic association: Derivation and evaluation by means of inverse temperature transitions, *Chem. Phys. Lett. 399*, 177−183.
52. Sandberg, L., and Edholm, O. (2001) Calculated solvation free energies of amino acids in a dipolar approximation, *J. Phys. Chem. B 105*, 273−281.
53. Perutz, M. F., Johnson, T., Suzuki, M., and Finch, J. T. (1994) Glutamine repeats as polar zippers: Their possible role in inherited neurodegenerative diseases, *Proc. Natl. Acad. Sci. U.S.A. 91*, 5355−5358.
54. Perutz, M. F., Staden, R., Moens, L., and Debaere, I. (1993) Polar zippers, *Curr. Biol. 3*, 249−253.
55. Perutz, M. F., Finch, J. T., Berriman, J., and Lesk, A. (2002) Amyloid fibers are water-filled nanotubes, *Proc. Natl. Acad. Sci. U.S.A. 99*, 5591−5595.
56. Perutz, M. F., Pope, B. J., Owen, D., Wanker, E. E., and Scherzinger, E. (2002) Aggregation of proteins with expanded glutamine and alanine repeats of the glutamine-rich and asparagine-rich domains of Sup35 and of the amyloid β-peptide of amyloid plaques, *Proc. Natl. Acad. Sci. U.S.A. 99*, 5596−5600.
57. Liu, Y. S., Gotte, G., Libonati, M., and Eisenberg, D. (2001) A domain-swapped RNAse A dimer with implications for amyloid formation, *Nat. Struct. Biol. 8*, 211−214.
58. Yoder, M. D., Lietzke, S. E., and Jurnak, F. (1993) Unusual structural features in the parallel β-helix in pectate lyases, *Structure 1*, 241−251.
59. Jenkins, J., Shevchik, V. E., Hugouvieux-Cotte-Pattat, N., and Pickersgill, R. W. (2004) The crystal structure of pectate lyase Pel9a from *Erwinia chrysanthemi*, *J. Biol. Chem. 279*, 9139−9145.
60. Thakur, A. K., and Wetzel, R. (2002) Mutational analysis of the structural organization of polyglutamine aggregates, *Proc. Natl. Acad. Sci. U.S.A. 99*, 17014−17019.
61. Wickner, R. B. (1994) URE3 as an altered Ure2 protein: Evidence for a prion analog in *Saccharomyces cerevisiae*, *Science 264*, 566−569.
62. Edskes, H. K., Gray, V. T., and Wickner, R. B. (1999) The URE3 prion is an aggregated form of Ure2p that can be cured by overexpression of Ure2p fragments, *Proc. Natl. Acad. Sci. U.S.A. 96*, 1498−1503.
63. Lacroute, F. (1971) Non-Mendelian mutation allowing ureidosuccinic acid uptake in yeast, *J. Bacteriol. 106*, 519−522.
64. Umland, T. C., Taylor, K. L., Rhee, S., Wickner, R. B., and Davies, D. R. (2001) The crystal structure of the nitrogen regulation fragment of the yeast prion protein Ure2p, *Proc. Natl. Acad. Sci. U.S.A. 98*, 1459−1464.
65. Taylor, K. L., Cheng, N. Q., Williams, R. W., Steven, A. C., and Wickner, R. B. (1999) Prion domain initiation of amyloid formation in vitro from native Ure2p, *Science 283*, 1339−1343.
66. Baxa, U., Speransky, V., Steven, A. C., and Wickner, R. B. (2002) Mechanism of inactivation on prion conversion of the *Saccharomyces cerevisiae* Ure2 protein, *Proc. Natl. Acad. Sci. U.S.A. 99*, 5253−5260.
67. Kajava, A. V., Baxa, U., Wickner, R. B., and Steven, A. C. (2004) A model for Ure2p prion filaments and other amyloids: The parallel superpleated β-structure, *Proc. Natl. Acad. Sci. U.S.A. 101*, 7885−7890.
68. Baxa, U., Cheng, N., Winkler, D. C., Chiu, T., Davies, D. R., Sharma, D., Inouye, H., Kirschner, D. A., Wickner, R. B., and Steven, A. C. (2005) Filaments of the Ure2p prion protein have a cross-β core structure, *J. Struct. Biol.* (in press).
69. Kishimoto, A., Hasegawa, K., Suzuki, H., Taguchi, H., Namba, K., and Yoshida, M. (2004) β-Helix is a likely core structure of yeast prion Sup35 amyloid fibers, *Biochem. Biophys. Res. Commun. 315*, 739−745.
70. Sieber, P., and Riniker, B. (1991) Protection of carboxamide functions by the trityl residue: Application to peptide-synthesis, *Tetrahedron Lett. 32*, 739−742.
71. Ishii, Y., Balbach, J. J., and Tycko, R. (2001) Measurement of dipole-coupled line shapes in a many-spin system by constant-time two-dimensional solid-state NMR with high-speed magic-angle spinning, *Chem. Phys. 266*, 231−236.
72. Gullion, T., and Schaefer, J. (1989) Rotational-echo double-resonance NMR, *J. Magn. Reson. 81*, 196−200.
73. Jaroniec, C. P., Tounge, B. A., Herzfeld, J., and Griffin, R. G. (2001) Frequency selective heteronuclear dipolar recoupling in rotating solids: Accurate ^{13}C-^{15}N distance measurements in uniformly ^{13}C,^{15}N-labeled peptides, *J. Am. Chem. Soc. 123*, 3507−3519.
74. Wagner, A., and Luger, P. (2001) Charge density and topological analysis of L-glutamine, *J. Mol. Struct. 595*, 39−46.
75. Sorensen, O. W., Eich, G. W., Levitt, M. H., Bodenhausen, G., and Ernst, R. R. (1983) Product operator formalism for the description of NMR pulse experiments, *Prog. Nucl. Magn. Reson. Spectrosc. 16*, 163−192.
76. Gullion, T., Baker, D. B., and Conradi, M. S. (1990) New, compensated Carr-Purcell sequences, *J. Magn. Reson. 89*, 479−484.
77. Bennett, A. E., Rienstra, C. M., Auger, M., Lakshmi, K. V., and Griffin, R. G. (1995) Heteronuclear decoupling in rotating solids, *J. Chem. Phys. 103*, 6951−6958.
78. Petkova, A. T., and Tycko, R. (2002) Sensitivity enhancement in structural measurements by solid-state NMR through pulsed spin locking, *J. Magn. Reson. 155*, 293−299.
79. Oas, T. G., Hartzell, C. J., McMahon, T. J., Drobny, G. P., and Dahlquist, F. W. (1987) The carbonyl ^{13}C chemical-shift tensors of five peptides determined from ^{15}N dipole-coupled chemical shift powder patterns, *J. Am. Chem. Soc. 109*, 5956−5962.

80. Koradi, R., Billeter, M., and Wuthrich, K. (1996) Molmol: A program for display and analysis of macromolecular structures, *J. Mol. Graphics 14*, 51−55.
81. Wishart, D. S., Bigam, C. G., Holm, A., Hodges, R. S., and Sykes, B. D. (1995) ^{1}H, ^{13}C, and ^{15}N random coil NMR chemical shifts of the common amino acids. 1. Investigations of nearest-neighbor effects, *J. Biomol. NMR 5*, 67−81.
82. Saito, H. (1986) Conformation-dependent ^{13}C chemical shifts: A new means of conformational characterization as obtained by high-resolution solid state ^{13}C NMR, *Magn. Reson. Chem. 24*, 835−852.
83. Spera, S., and Bax, A. (1991) Empirical correlation between protein backbone conformation and Cα and Cβ ^{13}C nuclear magnetic resonance chemical shifts, *J. Am. Chem. Soc. 113*, 5490−5492.
84. Wishart, D. S., Sykes, B. D., and Richards, F. M. (1991) Relationship between nuclear magnetic resonance chemical shift and protein secondary structure, *J. Mol. Biol. 222*, 311−333.
85. Long, H. W., and Tycko, R. (1998) Biopolymer conformational distributions from solid-state NMR: α-Helix and 3_{10}-helix contents of a helical peptide, *J. Am. Chem. Soc. 120*, 7039−7048.
86. Weliky, D. P., Bennett, A. E., Zvi, A., Anglister, J., Steinbach, P. J., and Tycko, R. (1999) Solid-state NMR evidence for an antibody-dependent conformation of the V3 loop of HIV-1 gp120, *Nat. Struct. Biol. 6*, 141−145.
87. Sharpe, S., Kessler, N., Anglister, J. A., Yau, W. M., and Tycko, R. (2004) Solid-state NMR yields structural constraints on the V3 loop from HIV-1 gp120 bound to the 447−52d antibody Fv fragment, *J. Am. Chem. Soc. 126*, 4979−4990.
88. Diaz-Avalos, R., Long, C., Fontano, E., Balbirnie, M., Grothe, R., Eisenberg, D., and Caspar, D. L. D. (2003) Cross-β order and diversity in nanocrystals of an amyloid-forming peptide, *J. Mol. Biol. 330*, 1165−1175.
89. Tycko, R., and Ishii, Y. (2003) Constraints on supramolecular structure in amyloid fibrils from two-dimensional solid-state NMR spectroscopy with uniform isotopic labeling, *J. Am. Chem. Soc. 125*, 6606−6607.
90. Jaroniec, C. P., MacPhee, C. E., Astrof, N. S., Dobson, C. M., and Griffin, R. G. (2002) Molecular conformation of a peptide fragment of transthyretin in an amyloid fibril, *Proc. Natl. Acad. Sci. U.S.A. 99*, 16748−16753.
91. Ross, E. D., Baxa, U., and Wickner, R. B. (2004) Scrambled prion domains form prions and amyloid, *Mol. Cell. Biol. 24*, 7206−7213.
92. Guo, J. T., Wetzel, R., and Ying, X. (2004) Molecular modeling of the core of Aβ amyloid fibrils, *Proteins 57*, 357−364.
93. Ma, B. Y., and Nussinov, R. (2002) Stabilities and conformations of Alzheimer's β-amyloid peptide oligomers ($A\beta_{16-22}$, $A\beta_{16-35}$, and $A\beta_{10-35}$): Sequence effects, *Proc. Natl. Acad. Sci. U.S.A. 99*, 14126−14131.
94. Smith, C. K., Withka, J. M., and Regan, L. (1994) A thermodynamic scale for the β-sheet forming tendencies of the amino acids, *Biochemistry 33*, 5510−5517.
95. Minor, D. L., and Kim, P. S. (1994) Measurement of the β-sheet-forming propensities of amino acids, *Nature 367*, 660−663.

BI050724T